Ordered Structure and Thermal Expansion in Tungsten Bronze Pb$_2$K$_{0.5}$Li$_{0.5}$Nb$_5$O$_{15}$

Kun Lin,[†] Yangchun Rong,[†] Hui Wu,[‡,§] Qingzhen Huang,[‡] Li You,[∥] Yang Ren,[⊥] Longlong Fan,[†] Jun Chen,[†] and Xianran Xing*,[†]

[†]Department of Physical Chemistry and [∥]State Key Laboratory for Advanced Metals and Materials, University of Science and Technology Beijing, Beijing 100083, China

[‡]Center for Neutron Research, National Institute of Standards and Technology (NIST), Gaithersburg, Maryland 20899-6102, United States

[§]Department of Materials Science and Engineering, University of Maryland, College Park, Maryland 20742-2115, United States

[⊥]X-ray Science Division, Argonne National Laboratory, Argonne, Illinois 60439, United States

S *Supporting Information*

ABSTRACT: The crystal structure and thermal expansion behaviors of a new tetragonal tungsten bronze (TTB) ferroelectric, Pb$_2$K$_{0.5}$Li$_{0.5}$Nb$_5$O$_{15}$, were systematically investigated by selected-area electron diffraction (SAED), neutron powder diffraction, synchrotron X-ray diffraction (XRD), and high-temperature XRD. SAED and Rietveld refinement reveal that Pb$_2$K$_{0.5}$Li$_{0.5}$Nb$_5$O$_{15}$ displays a commensurate superstructure of simple orthorhombic TTB structure at room temperature. The structure can be described with space group $Bb2_1m$. The transition to a paraelectric phase ($P4/mbm$) occurs at 500 °C. Compared with Pb$_2$KNb$_5$O$_{15}$ (PKN), the substitution of 0.5K$^+$ with small 0.5Li$^+$ into PKN causes the tilting of NbO$_6$ octahedra away from the c axis with $\Delta\theta \approx 10°$ and raises the Curie temperature by 40 °C, and the negative thermal expansion coefficient along the polar b axis increases more than 50% in the temperature range 25−500 °C. We present that, by introduction of Li$^+$, the enhanced spontaneous polarization is responsible for the enhanced negative thermal expansion along the b axis, which may be caused by more Pb^{2+} in the pentagonal caves.
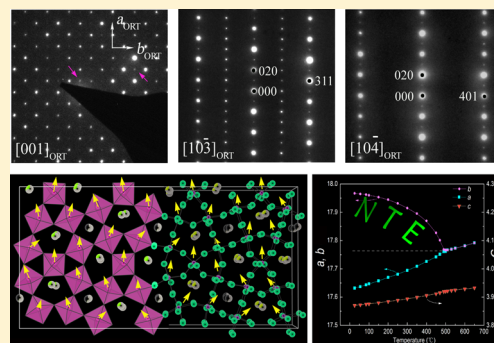
INTRODUCTION

Tetragonal tungsten bronze (TTB) niobates are one large type of complex structures that have been widely investigated. Sr$_x$Ba$_{1-x}$Nb$_2$O$_6$ (Sr$_{5x}$Ba$_{5-5x}$Nb$_{10}$O$_{30}$, 0.25 ≤ x ≤ 0.75, abbreviated as SBN), as an example, shows excellent electro-optic, pyroelectric, dielectric, and nonlinear-optical properties.[1−3] A giant electrocaloric effect was detected in the SBN film, implying that TTB niobates may be appreciable candidates in refrigeration.[1] The basic skeletons of TTB niobates are composed of stable corner-sharing NbO$_6$ octahedra forming three different tunnels: one containing quadrangular 12-coordinated A1 sites, one containing pentagonal 15-coordinated A2 sites, and one small triangular tunnel containing 9-coordinated A3 sites, which can be filled with very small ions such as Li$^+$ ions (see Figure S1 in the Supporting Information, SI). The ideal TTB compounds have the general formula (A2)$_4$(A1)$_2$(A3)$_4$ (B1)$_2$(B2)$_8$O$_{30}$, where B sites are often occupied by Nb^{5+}, Ta^{5+}, etc. Because of its great flexibility in composition, diversity in both the structures and properties of TTB materials can be achieved.

A number of relaxor ferroelectrics were found in TTB niobates. The relaxation behaviors in TTB could originate from the structural disorder in both A and B sites. Ba$_6$M^{3+}Nb$_9$O$_{30}$ (M = Ga^{3+}, Sc^{3+}, In^{3+}, or Co^{3+}) are relaxors with the dipole moment restricted to the B1 sites.[4,5] In Ba$_2$MTi$_2$Nb$_3$O$_{15}$ (M = Bi^{3+}, La^{3+}, Nd^{3+}, Sm^{3+}, Gd^{3+}),[6] with a decrease of the M cation size, the materials change from relaxation ferroelectrics (Bi^{3+}, La^{3+}) to classical ferroelectrics (Nd^{3+}, Sm^{3+}, Gd^{3+}), which is related to the degree of chaos in the A1 and A2 sites. The occupancies of different tunnels and octahedra strongly influence their physics properties as well as the crystal structures.

Among the TTB ferroelectrics, Pb-based niobates have high Curie temperatures (T_C) and well electric properties.[7,8] Lead potassium niobate (Pb$_2$KNb$_5$O$_{15}$, PKN for short; T_C = 460 °C) is a good example with well ferroelectric, dielectric, and optical properties.[9−11] Both the structural and ferroelectric aspects have been widely studied.[9−11,13] In our previous study,[14] we reported the abnormal thermal expansion behavior in PKN. Below the Curie temperature, the lattice constant b (polar axis) decreases abnormally with an increase of the temperature. It is known in PKN that the thermal contraction along the b axis is closely related to Pb atoms with lone-pair electrons, especially in the large pentagonal caves. Because the small Li$^+$ ions can

move to the A3 sites, substitution with Li$^+$ could introduce vacancies into the A1 and A2 sites and change the chemical environment significantly. In order to advance the knowledge of the influence of Pb^{2+} in the crystal structure, thermal expansion, and physical properties in TTB niobates, equivalent substitution of 0.5K$^+$ with 0.5Li$^+$ was performed. In this study, we carried out a detailed structure and physical property study of Pb$_2$K$_{0.5}$Li$_{0.5}$Nb$_5$O$_{15}$ (PKLN) by means of high-resolution neutron powder diffraction (NPD), high-energy synchrotron X-ray radiation, high-temperature X-ray diffraction (HTXRD), and selected-area electron diffraction (SAED). We confirmed the commensurate superstructure nature of PKLN with both *a* and *c* axes doubled in dimension, which would be related to the ordering of ions in the A sites by the introduction of vacancies.

■ EXPERIMENTAL DETAILS

Samples were synthesized by a solid-state method[14] with starting materials PbO, K$_2$CO$_3$, Li$_2$CO$_3$, and Nb$_2$O$_5$. The ball-milled powders were sintered at 800 °C for 2 h and 1200 °C for 2 h with intermediate grinding. Mass loss in the sintering process just matches decomposition of the carbonates. NPD data were collected on the BT-1 diffractometer at the Center for Neutron Research at the NIST with a Cu monochromator (λ = 1.5403 Å) at room temperature (RT). High-energy synchrotron powder diffraction was performed at RT at beamline 11-ID-C at the Advanced Photon Source. The wavelength of synchrotron light was 0.111538 Å. HTXRD (X'Pert^3 Powder, PANalytical,[15] Holland, Cu Kα, λ = 1.5406 Å) data were collected from RT to 650 °C. The heating rate was 10 °C/min, and the sample was held for 10 min at a specified temperature to reach heat equilibrium. For SAED experiments, a pellet specimen was pretreated with ion-beam thinning. SAED was performed on a Tecnai G2 F30 S-TWIN transmission electron microscope with an accelerating voltage of 300 kV. Dielectric parameters of unpoled samples were measured as a function of the frequency and temperature with an impedance analyzer (HP4192A; Hewlett-Packard, Palo Alto, CA) in the frequency range of 10^2–10^6 Hz. Some powder samples were dissolved in a hydrofluoric acid solution for chemical composition determination using inductively coupled plasma optical emission spectroscopy (ICP-OES; Thermo IRIS Intrepid II). The cation ratio is Pb$_{1.95}$K$_{0.48}$Li$_{0.50}$Nb$_5$ (error <5%), suggesting that the sample is stoichiometric.

■ RESULTS AND DISCUSSION

Structure Determination. High-resolution NPD, high-energy synchrotron XRD, and the Rietveld method were carried out to study the RT structure. The model *Cm2m* (space group for PKN) can fit the synchrotron XRD well (see Figure S2 in the SI); however, a poor fit to the NPD pattern occurs ($R_{wp} \approx$ 9.29 and χ^2 = 6.49; see Figure 1a). In addition, very weak peaks with intensities of less than 1% in the low-angle region of the synchrotron XRD pattern can be distinguished clearly above the smooth background, which is not observed in PKN (Figure S3 in the SI) and cannot be indexed by the *Cm2m* space group (Figure 2). According to the literature, such weak peaks could be caused by the superstructure of TTB structures.[16,17] Because neutron scattering is more sensitive to light O atoms than X-ray scattering, the discrepancies in the NPD fitting may be caused by NbO$_6$ octahedra tilting.[18] Some of these peaks can also coincide with raw materials PbO (PDF 5-561) and Nb$_2$O$_5$ (PDF 74-298), but it is unclear.

A transmission electron microscopy (TEM) study was carried out to further study the microstructure of PKLN. Parts a−c of Figure 3 show the SAED patterns along different zone axes. In Figure 3a−c, the main reflection spots represent the reflection spots of the *Cm2m* model. The existence of weak reflections in Figure 3a (pink arrows) confirms the deviation
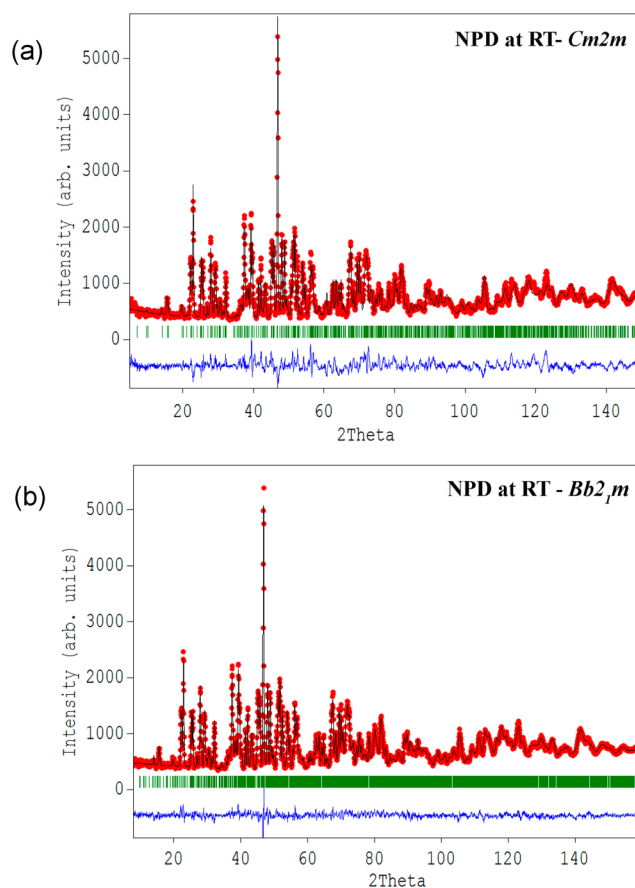
Figure 1. Rietveld refinement of PKLN on the NPD pattern using space groups (a) *Cm2m* and (b) *Bb2$_1$m*.

from the *Cm2m* model. Tilting the sample around the *b*$_{ort}$ directions results in a series of patterns (see Figure 3b,c). In these patterns, the main reflection spots are consistent with the *Cm2m* model corresponding to [10$\bar{3}$] and [10$\bar{4}$] zone axes, respectively (see Figure 3d−f). The crystal indices (*h*/2, *k*, *l*/2) in Figure 3b indicate the doubling of cell parameters *a* and *c* (*a* = 2*a*$_{ort}$ ≈ 35 Å, *b* = *b*$_{ort}$ ≈ 17 Å, and *c* = 2*c*$_{ort}$ ≈ 8 Å). The diffraction conditions are compatible with noncentrosymmetric space groups *Bbm*2 (No. 40), *Bb2$_1$m* (No. 36), and *B22$_1$2* (No. 20) and centrosymmetric space group *Bbmm* (No. 63). Considering the measured ferroelectric hysteresis loop in the material (see Figure S4 in the SI), only the polar *Bbm*2 and *Bb2$_1$m* are taken into account. These two space groups have different polar axis directions.

On the basis of our previous study and the structural references in the literature,[14,19,20] the polarization directions of ferroelectric TTB structures are divided into two types: along the stacking direction of the NbO$_6$ layers (*c*-axis direction) or within the NbO$_6$ layer (*b*-axis direction). The latter case only occurs in several compounds that contain enough Pb in the A sites, such as PKN,[21,12,14] Pb$_2$NaNb$_5$O$_{15}$,[19] Pb$_{1-x}$Ba$_x$Nb$_2$O$_6$ (*x* < 0.3),[22] Pb$_{2(1-x)}$K$_{1+x}$Gd$_x$Nb$_5$O$_{15}$ (*x* < 0.2),[23] and PbNb$_2$O$_6$.[20,24] In Pb$_{1-x}$Ba$_x$Nb$_2$O$_6$ and Pb$_{2(1-x)}$K$_{1+x}$Gd$_x$Nb$_5$O$_{15}$, with a decrease of the Pb content, the spontaneous polarization direction changes from the *b* axis to the *c* axis. The case of PKLN is similar to those above. On the other hand, abnormal thermal expansion in ferroelectrics usually occurs along the polar direction. In PbTiO$_3$-based compounds, negative thermal expansion (NTE) occurs in the polar *c* direction.[25−27] In the
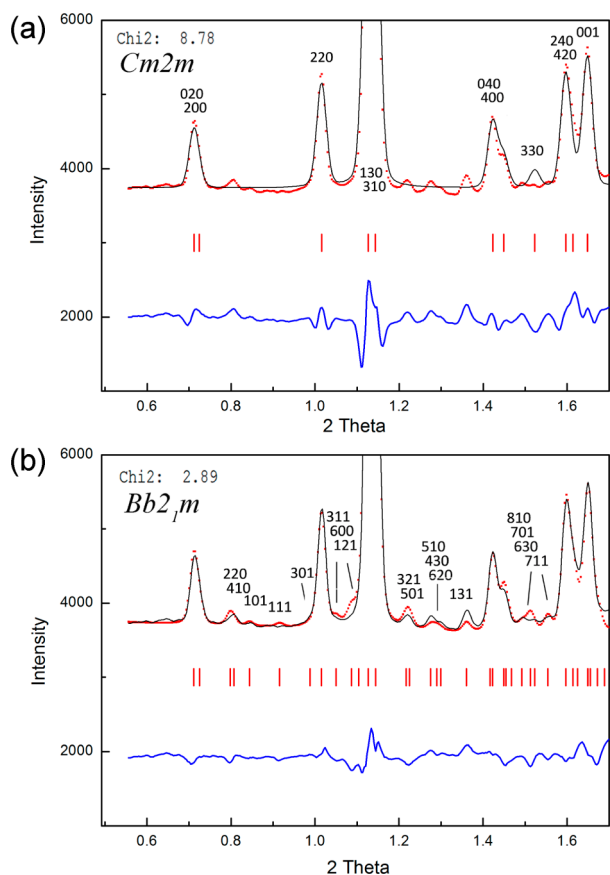
Figure 2. Low-angle region of the RT synchrotron XRD pattern of PKLN refined according to space groups $Cm2m$ (a) and $Bb2_1m$ (b) in the range of $0.6 < 2\theta < 1.7°$ (3.76 Å < d < 10.6 Å). Observed (red dots), calculated (black curve), and difference (blue curve in the bottom) intensities and Bragg reflections (red bars) are shown. Part a shows the Miller indices corresponding to $Cm2m$. The extra reflections that do not belong to $Cm2m$ can be indexed with $Bb2_1m$ in part b.

TTB structure $Sr_xBa_{1-x}Nb_2O_6$ ($x = 0.75$), slight NTE was reported along the c axis,[28,29] which is also the polar direction. A similar result is also observed along the b axis of PKLN (discussed below). On the basis of these facts, we adopt space group $Bb2_1m$ with the polar axis direction along the b axis. Parts

g−i of Figure 3 show the simulated electron diffractions of the structure with space group $Bb2_1m$. The experimental SAED patterns can match the simulated ones. Note that in Figure 3b,c the weak reflections located at $(0k0)$ $(k = 2n + 1)$ are caused by the double-diffraction effect.

The doubling of the unit cell dimensions can be viewed as a commensurate superstructure of the basic cell.[16,17,30] Crystals with superstructures are often caused by periodic composition fluctuation or the ordering of atomic positional arrangement.[31,32] The formation of superstructures usually demands long time heat treatment (dozens of hours or more) at high temperatures to reach dynamic conditions.[16,17,30] In this study, the commensurate superstructure nature in PKLN was observed and was synthesized in only 2 h. With similar synthesis conditions (compared to PKN), the appearance of a superstructure in PKLN suggests its special structural features. In PKN, all of the pentagonal (15-coordinated) and quadrangular (12-coordinated) caves are fully occupied and the atomic positions in pentagonal caves split,[12,14] while in the TTB structure of PKLN, the smaller triangular caves (9-coordinated) can only be occupied by very small ions such as Li^+,[33−35] and the equivalent substitution of $0.5K^+$ with $0.5Li^+$ could introduce vacancies into both pentagonal and quadrangular caves. Therefore, the arrangement of the PKLN structure is very intriguing.

The combination of NPD and synchrotron XRD patterns at RT is used to refine the structure simultaneously on the platform of software $Fullprof^{36}$ and $PowderX.^{37}$ Figures 1b and S2 in the SI show the refinement patterns, and good agreement between the observed and calculated patterns was observed. The refined structural parameters and crystal structure are shown in Table 1 and Figure 4.

In the refinement process, the possible distributions of K^+ and Pb^{2+} in different A sites, which have a strong influence on the calculated structure factors, were tested. The occupancy of K in A1 sites converged to be a little negative (about −5%) and was then set as zero, which means that K occupies the A2 sites only. The A2 sites are occupied by 74.4(0)% Pb and 25% K, and the A1 sites are only occupied by 51.1(0)% Pb. The total occupying ratio in the A2 sites is almost 100% (99.4%), which implies a strong preference to occupy the larger pentagonal tunnels for both Pb^{2+} and K^+ cations. Compared to Pb^{2+}, K^+
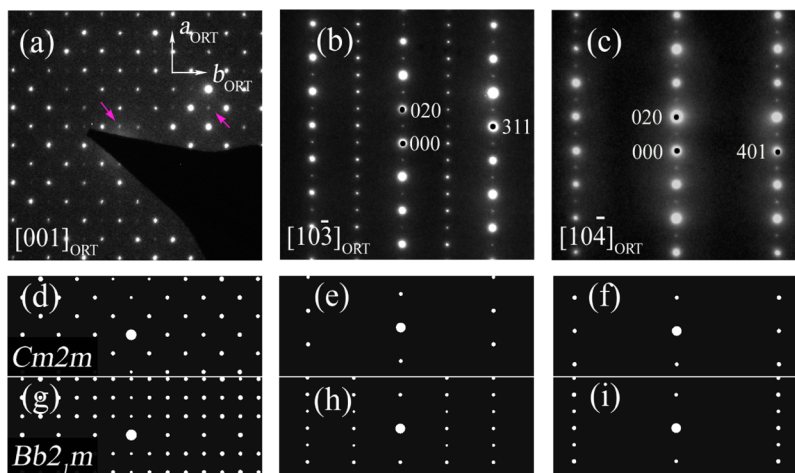
Figure 3. (a−c) Electron diffraction patterns obtained along different zone axes. The hkl indices are indexed using the $Cm2m$ model. Parts d−f and g−i are electron diffractions simulated corresponding zone axes of PKLN with space groups $Cm2m$ and $Bb2_1m$.

Table 1. Crystallographic Data of PKLN Refined from Neutron and Synchrotron XRD Data at RT

	NPD	synchrotron XRD
R_p	3.93	1.63
R_{wp}	5.1	2.17
R_{exp}	3.64	1.27
χ^2	1.96	2.92
space group		$Bb2_1m$ (No. 36)
a		35.2811(3)
b		17.9662(1)
c		7.7497(1)
15-coordinated site occupancy (A2)		74.4% Pb, 25% K
12-coordinated site occupancy (A1)		51.1% Pb

Figure 4. *ab* projection of the unit cell of PKLN. The left side shows in A-site atoms and NbO_6 octahedra. The right side shows in a ball-and-stick model. The Li atoms are omitted.

Figure 5. Presentation of the ordering of A-site atoms along the *c* axis at RT. In PKLN (a), there are not splits, but the atoms have different positions in different layers. In PKN (b), the atoms in the 15-coordinated site split into different positions in each layer.

seems to have the priority to occupy the A2 sites, and then Pb^{2+} "goes into" the rest of the A2 sites, leaving the rest of Pb^{2+} in the smaller quadrangular tunnels. Considering the larger ionic radius of K^+ (1.64 Å, CN = 12) than Pb^{2+} (1.49 Å, CN = 12),[38] such an occupying sequence seems to be dominated by the cation radius. Just as the case in PKN, K only occupies the A2 sites, and Pb occupies A1 and the rest of the A2 sites.[12] This study excludes the small Li^+ from the largest pentagonal caves (A2).

Attempts to identify the accurate position of Li^+ were unsuccessful because of its weak scattering ability. At the end of refinement, insertion of Li^+ into A3 or the rest of the A1 sites did not obviously reduce the R factors (about 1%), but the positions of Li^+ cannot converge to reasonable positions. Thus, the Li^+ position in the structure was not described. Both the triangular A3 sites and quadrangular A1 sites may have Li^+, but it is unclear based on the current data. The final atomic positions are shown in the CIF files in the SI.

Figure 4 shows the structure of PKLN at RT. The unit cell is composed of four orthorhombic cells. In PKN, Pb and K have different positions in the same A2 sites with a distance of about 0.5 Å.[12,14] In addition, the Pb atoms themselves split into pairs on two disorder positions in the same A2 sites, which was also observed in $Pb_2KTa_5O_{15}$,[39] while in the structure of PKLN, A-site atoms have different positions (at different layers) viewed down the *c* axis (Figure 4) and the atoms did not split during the refinement. Compared with the 12-coordinated sites, the atoms in the 15-coordinated sites separate into two sets of alternating sites with much longer A–B distances in the projection plane (Figure 4). The results are consistent with the commensurate superstructure with *c* doubled; see Figure 5. Figure 5 also illustrates the structure of PKN for comparison, where A sites only show splitting within each layer. In that

sense, the commensurate superstructure of PKLN can be viewed as a result of A-site cation ordering (especially in the 15-coordinated A2 sites, namely, A–B–A–B). The differences in the occupancies between A and B or C and D in Figure 5a are not refined in this study because of the limitation of the present data.

Attention is turned to the simulated SAED patterns compared with the experimental ones, shown in Figure 3. The absence of alternately dark and bright intensities in the simulated reflection of the $Bb2_1m$ model suggests the presence of extra ordering in the real lattice. The samples are synthesized in only 2 h, indicating a strong tendency for Pb and K to get ordered. It seems that the vacancies in the 12- or 15-coordinated sites, introduced by substitution with Li^+, provide Pb^{2+} and K^+ enough space to better accommodate their positions in the three-dimensional tunnels.

Furthermore, substitution with Li^+ changes the behaviors of NbO_6 octahedra as well. In PKN, there is no tilt of NbO_6 octahedra along the *c* axis; however, obvious tilt was observed in PKLN (see Figure 5a) accompanied by the doubling of cell parameters *c*. The average tilt angle is $\theta \approx 10°$ (see Table S1 in the SI). The relationship between the occupation in the A site and the tilt of NbO_6 octahedra requires further investigation.

The structure refinement of PKLN at 550 °C was performed by the Rietveld method using XRD data. The experimental, calculated, and difference profiles are shown in Figure 6. Fractional coordinates are given according to the basic TTB structure with centrosymmetric space group $P4/mbm$ (No. 127). The unit cell dimension is about 12 Å × 12 Å × 4 Å. The existence of K^+ in the A1 sites was excluded in the refining process. The prolate anisotropic thermal factors indicate the split of Pb in the A2 sites (see Figure S6 in the SI). Table 2 summarizes the crystallographic parameters of PKLN at 550 °C. The final site occupancies are almost the same as those at RT, which may be due to the absence of diffusion below 550 °C.

The temperature dependence of relative dielectric constant and loss is shown in Figure 7. Only one peak can be distinguished from RT to 650 °C. The transition from the ferroelectric phase to the paraelectric phase occurs at about 500 °C. The dielectric maximum temperature T_{max} is almost unchanged with increasing frequency from 10^2 to 10^6 Hz (from 498 to 502 °C), implying a classical ferroelectric phase

9177

dx.doi.org/10.1021/ic501189n | *Inorg. Chem.* 2014, 53, 9174–9180

Figure 6. Rietveld fit of the powder XRD pattern of PKLN collected at 550 °C with space group $P4/mbm$.

Table 2. Crystallographic Data of PKLN Refined from XRD Collected at 550 °C

	XRD (550 °C)
R_p	2.66
R_{wp}	3.83
R_{exp}	2.01
χ^2	3.63
space group	$P4/mbm$ (No. 127)
a	12.5667(0)
b	12.5667(0)
c	3.92491(0)
15-coordinated site occupancy (A2)	74.8% Pb, 25% K
12-coordinated site occupancy (A1)	50.9% Pb

transition behavior. The absence of relaxor phenomena excludes strong disorder in the same A cave, which agrees with our structure discussion.

Thermal Expansion. High-temperature XRD measurement from RT to 650 °C was used to study the thermal expansion behaviors of PKLN (Figure S7 in the SI). Temperature dependence of cell parameters is shown in Figure 8a,b. For comparison, parameters a and c are fitted to a simple orthorhombic unit cell ($a_{ort} \times b_{ort} \times c_{ort}$). It is clearly shown that the structure transforms from the orthorhombic phase to the tetragonal phase at $T_C \approx 500$ °C, which is consistent with the dielectric measurement (Figure 7). The cell parameters a and c increase with temperature, while b decreases. NTE was observed along the b axis from RT to about 500 °C.

The comparison with PKN is shown in Figure 8c−e and Table 3. Figure 8c shows the temperature dependence of relative cell parameters. We can see that the anisotropy of thermal expansion is enhanced after the substitution of K$^+$ with Li$^+$. The negative thermal expansion coefficient (TEC) along the b axis is enhanced by 50% (from -1.56×10^{-5} °C^{-1} for PKN to -2.36×10^{-5} °C^{-1} for PKLN), while the positive TEC along the c direction is increased by 68% (from 1.62×10^{-5} °C^{-1} for PKN to 2.73×10^{-5} °C^{-1} for PKLN), giving rise to a total volumetric thermal expansion increased from 1.35×10^{-5} °C^{-1} for PKN to 1.97×10^{-5} °C^{-1} for PKLN; see Figure 8c,d and Table 3. In orthorhombic phase of TTB, orthorhombic distortion (axis ratio b/a) is introduced to describe the degree of deviation from the tetragonal phase. The temperature dependence of b/a is shown in Figure 8e. For both PKLN and PKN, b/a gradually decreases to 1, and the value of b/a for
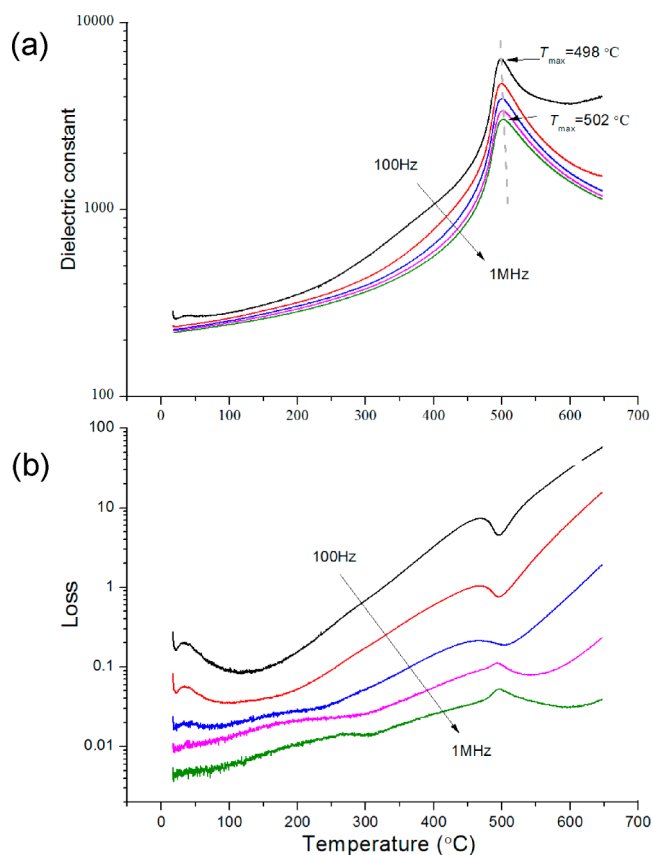
Figure 7. Temperature dependence of relative dielectric constant (a) and loss (b) of PKLN in the frequency range of 10^2-10^6 Hz. The dielectric maximum temperature T_{max} did not show an obvious frequency dependence, implying a classic ferroelectric phase transition.

PKLN is 50% larger than that of PKN below T_C. The increase of b/a is consistent with the increase of the Curie temperature (460 °C for PKN and 500 °C for PKLN), indicating stronger spontaneous polarization (P_S) in PKLN. Because of the uncertainty of the Li atomic positions, the P_S value is not calculated.

In PKN, the spontaneous polarization is closely related to b/a and the negative TEC along the b direction,[14] similar to c/a in perovskites.[25−27] With increasing temperature, the release of ferroelectric interaction leads to the distortion and cooperative rotation of NbO$_6$ octahedra, resulting in contraction of the polar b axis (see Figure 4b). The ferroelectric displacement motivated by spontaneous polarization tends to drag cations and anions along different directions parallel to P_S, which would induce large b/a. The Pb in the A sites can greatly enhance spontaneous polarization by Pb−O covalence (hybridization between the Pb 6s and O 2p states).[40,41] Higher Pb content will generate larger P_S (e.g., in PbTiO$_3$-related compounds[25−27]). In this study, spontaneous polarization is also enhanced by replacing of 0.5K$^+$ with 0.5Li$^+$, while keeping the total amounts of Pb unchanged. With the same amount of Pb in PKLN, 74% Pb atoms distribute in 15-coordinated sites and 26% in 12-coordinated sites, in sharp contrast to those in PKN with 50% in 15-coordinated sites and 50% in 12-coordinated sites.[14] This agrees with our previous suggestion, proposed in PKN,[14] that the Pb−O covalence in the 15-coordinated sites may have larger contribution to the spontaneous polarization because of its larger space allowing Pb^{2+} to accommodate a better coordinated environment.[14] On the other hand, the smaller
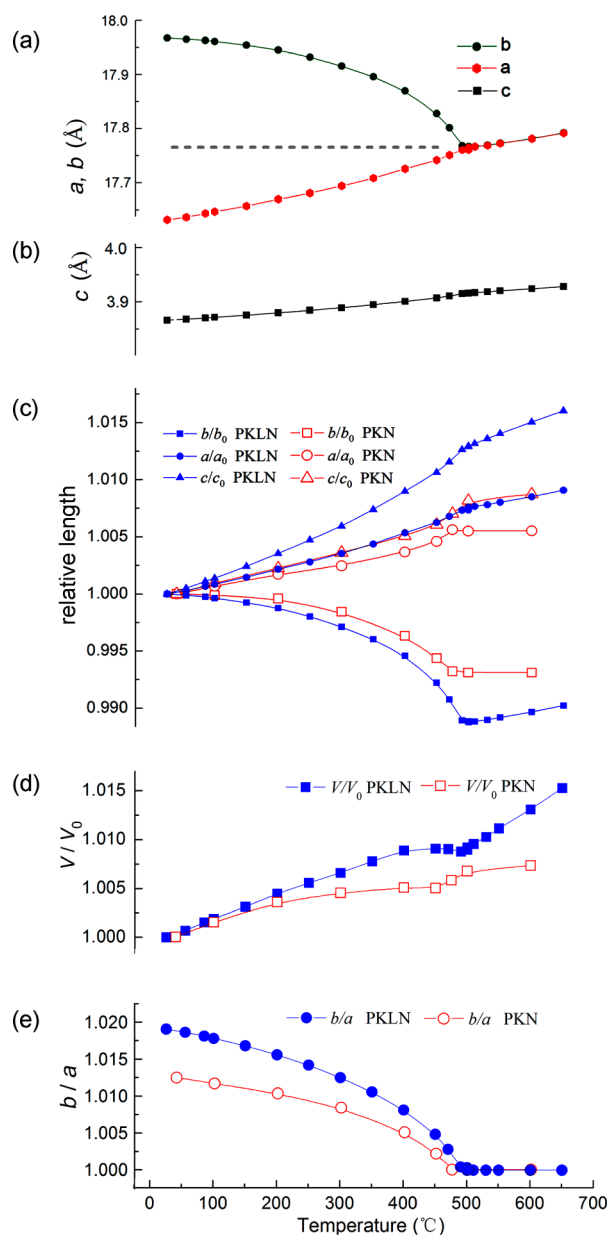
Figure 8. (a and b) Temperature dependence of cell parameters of PKLN measured by high-temperature XRD. Cell parameters a and c are fitted to the simple orthorhombic unit cell for comparison. (c and d) Temperature dependence of relative cell parameters and volumes of PKLN (blue, solid) compared with those of PKN (red, hollow). (e) Temperature dependence of orthorhombic distortion b/a of PKLN (blue, solid) compared with that of PKN (red, hollow). Error bars are too small to be distinguished.

Table 3. Average Thermal Expansion Coefficients along Different Directions Obtained from High-Temperature XRD

	$T_C/$ °C	temp range	$\alpha_b/10^{-5}$ °C^{-1}	$\alpha_a/10^{-5}$ °C^{-1}	$\alpha_c/10^{-5}$ °C^{-1}	$\alpha_V/10^{-5}$ °C^{-1}
PKN	460	RT to T_C	−1.56(0)	1.69(0)	1.62(0)	1.35(0)
PKLN	500	RT to T_C	−2.36(1)	1.60(0)	2.73(1)	1.97(2)
		$T > T_C$	0.97(1)	0.97(1)	2.06(0)	4.01(2)

Li$^+$ ions could reduce the short-range ionic repulsive force, which, on the contrary, contributes to long-range ferroelectric force.[40]

In PKLN, in addition, the NbO$_6$ octahedra tilt from the c axis by about 10°. As is shown in Figure 9a, the bond angle of O1−
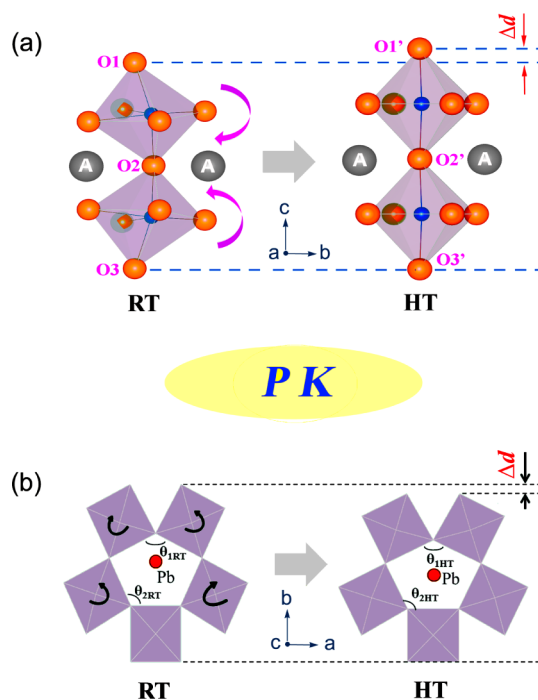
Figure 9. (a) Schematic presentation of NbO$_6$ octahedra tilting in the bc plane in PKLN from RT to 550 °C, which results in the extra positive thermal expansion along the c axis. The bond angle of O1−O2−O3 ranges from 153.6° to 169.1°, with an average of 160.12°, and the bond angle of O1′−O2′−O3′ is 180°. The average bond length of O1−O2 or O2−O3 is 3.96 Å, and the average bond length of O1′−O2′ or O2′−O3′ is 3.92 Å. (b) Octahedra cooperative rotation associated with Pb−O covalence, which accounts for NTE along the b axis.[14] The total volumetric TECs are mainly determined by the combined effect.

O2−O3 ranges from 153.6° to 169.1° with an average of 160.12° at RT (see Table S1 in the SI), which increases to 180° above T_C accompanied by the rapid elongation of the c axis. As a result, a sharp positive thermal expansion along the c direction was observed (Figure 3). The replacement of 0.5K$^+$ with 0.5Li$^+$ in PKN not only increases the axis ratio (b/a) but also induces the tilting of NbO$_6$ octahedra. It is interesting that the former enhances NTE along the polar b axis but the latter causes extra positive thermal expansion along the c axis. The bulk thermal expansion behavior will finally be determined by the combined effect of the two interactions. In the Pb$_2$MNb$_5$O$_{15}$ system, volumetric NTE may emerge if, by some chemical modulation, the polarization along the b axis is enhanced with NbO$_6$ octahedra untilt.

■ CONCLUSIONS

In conclusion, the commensurate superstructure feature of ferroelectric PKLN is observed at RT, which is associated with the cation ordering in A sites (especially 15-coordinated sites). By the introduction of small 0.5Li$^+$ into PKN, more Pb^{2+} occupy the large pentagonal caves and the Curie temperature increases by 40 °C. NTE along the polar b axis is enhanced by

more than half. The volumetric positive thermal expansion is also enhanced because of the tilt of NbO_6 octahedra.

Owning to the complexity of the RT structure of PKLN, we cannot guarantee absolute accuracy. On the basis of our study, the $Bb2_1m$ phase is the nearest model to describe the structure of the PKLN compound. This study gives further insight into the structural and thermal expansion features of TTB oxides at the atomic level. The mechanism will be helpful to understand the structure−property relationship of complex polyhedral framework ferroelectrics and can be used to design the thermomechanical properties of functional materials.

■ ASSOCIATED CONTENT

Ⓢ Supporting Information

Structure models, Rietveld refinement patterns of PKLN on a synchrotron XRD pattern, comparison of the synchrotron XRD for PKN and PKLN measurements at the same conditions, ferroelectric hysteresis loop, high-temperature XRD patterns, selected bond lengths and bond angles, and CIF files. This material is available free of charge via the Internet at http://pubs.acs.org.

■ AUTHOR INFORMATION

Corresponding Author
*E-mail: xing@ustb.edu.cn.

Notes
The authors declare no competing financial interest.

■ ACKNOWLEDGMENTS

■ REFERENCES

(1) Hamad, M. A. *Appl. Phys. Lett.* **2012**, *100*, 192908−4.
(2) Glass, A. M. *J. Appl. Phys.* **1969**, *40*, 4699−4713.
(3) Lee, S.; Wilke, R. H. T.; Trolier-McKinstry, S.; Zhang, S.; Randall, C. A. *Appl. Phys. Lett.* **2010**, *96*, 031910−3.
(4) Arnold, D. C.; Morrison, F. D. *J. Mater. Chem.* **2009**, *19*, 6485−6488.
(5) Rotaru, A.; Arnold, D. C.; Daoud-Aladine, A.; Morrison, F. D. *Phys. Rev. B* **2011**, *83*, 184302−12.
(6) Stennett, M. C.; Reaney, I. M.; Miles, G. C.; Woodward, D. I.; West, A. R.; Kirk, C. A.; Levin, I. *J. Appl. Phys.* **2007**, *101*, 104114−7.
(7) Goodman, G. *J. Am. Ceram. Soc.* **1953**, *36*, 368−372.
(8) Francombe, M. H.; Lewis, B. *Acta Crystallogr.* **1958**, *11*, 696−703.
(9) Subbarao, E. C.; Shirane, G. *J. Chem. Phys.* **1960**, *32*, 1846−1851.
(10) Nakano, J. I.; Yamada, T. *J. Appl. Phys.* **1975**, *46*, 2361−2365.
(11) Yamauchi, H. *Appl. Phys. Lett.* **1978**, *32*, 599−600.
(12) Sciau, P.; Calvarin, G.; Ravez, J. *Acta Crystallogr., Sect. B: Struct. Sci.* **1999**, *55*, 459−466.
(13) Belboukhari, A.; Abkhar, Z.; Choukri, E.; Gagou, Y.; Abdelmoula, N.; Elmoznine, R.; Mezzane, D.; Khemakhem, H.; Marssi, M. E.; Razumnaya, A.; Raevski, I.; Luk'yanchuk, I. *Ferroelectrics* **2013**, *444*, 116−124.
(14) Lin, K.; Wu, H.; Wang, F.; Rong, Y.; Chen, J.; Deng, J.; Yu, R.; Fang, L.; Huang, Q.; Xing, X. *Dalton Trans.* **2014**, *43*, 7037−7043.
(15) Certain commercial suppliers are identified in this paper to foster understanding. Such identification does not imply recommendation or endorsement by the NIST.
(16) García-González, E.; Torres-Pardo, A.; Jiménez, R.; González-Calbet, J. M. *Chem. Mater.* **2007**, *19*, 3575−3580.
(17) Torres-Pardo, A.; Jimenez, R.; Gonzalez-Calbet, J. M.; Garcia-Gonzalez, E. *Inorg. Chem.* **2011**, *50*, 12091−12098.
(18) There is no tilt of NbO_6 octahedra in the *Cm2m* model; see Figure S5 in the SI.
(19) Ravez, J.; Elouadi, B. *Mater. Res. Bull.* **1975**, *10*, 1249−1254.
(20) Labbé, P.; Frey, M.; Raveau, B.; Monier, J. C. *Acta Crystallogr., Sect. B: Struct. Sci.* **1977**, *33*, 2201−2212.
(21) Yamada, T. *Appl. Phys. Lett.* **1973**, *23*, 213−214.
(22) Venet, M.; Zabotto, F. L.; Eiras, J. A.; Garcia, D. *J. Appl. Phys.* **2009**, *105*, 124106−6.
(23) Amira, Y.; Gagou, Y.; Menny, A.; Mezzane, D.; Zegzouti, A.; Elaatmani, M.; El-Marssi, M. *Solid State Commun.* **2010**, *150*, 419−423.
(24) Labbe, P.; Frey, M.; Allias, G. *Acta Crystallogr., Sect. B: Struct. Sci.* **1973**, *29*, 2204−2210.
(25) Chen, J.; Nittala, K.; Forrester, J. S.; Jones, J. L.; Deng, J.; Yu, R.; Xing, X. *J. Am. Chem. Soc.* **2011**, *133*, 11114−11117.
(26) Chen, J.; Xing, X.; Sun, C.; Hu, P.; Yu, R.; Wang, X.; Li, L. *J. Am. Chem. Soc.* **2008**, *130*, 1144−1145.
(27) Chen, J.; Fan, L.; Ren, Y.; Pan, Z.; Deng, J.; Yu, R.; Xing, X. *Phys. Rev. Lett.* **2013**, *110*, 115901−5.
(28) Qadri, S. B.; Bellotti, J. A.; Garzarella, A.; Wu, D. H. *Appl. Phys. Lett.* **2005**, *86*, 251914−3.
(29) Gao, C. Y.; Xia, H. R.; Xu, J. Q.; Zhou, C. L.; Zhang, H. J.; Wang, J. Y. *Mater. Lett.* **2009**, *63*, 139−141.
(30) Mori, S.; Yamamoto, N.; Koyama, Y.; Uesu, Y. *Phys. Rev. B* **1997**, *55*, 11212−11217.
(31) Wolff, P. M. *Acta Crystallogr., Sect. A* **1974**, *30*, 777−785.
(32) Righi, L.; Albertini, F.; Pareti, L.; Paoluzi, A.; Calestani, G. *Acta Mater.* **2007**, *55*, 5237−5245.
(33) Gagou, Y.; Muller, C.; Frémy, M. A.; Mezzane, D.; Elkaïm, E.; Saint-Grégoire, P. *Phys. Status Solidi B* **2004**, *241*, 2629−2638.
(34) Kuang, X.; Pan, F.; Cao, J.; Liang, C.; Suchomel, M. R.; Porcher, F.; Allix, M. *Inorg. Chem.* **2013**, *52*, 13244−13252.
(35) Prades, M.; Maso, N.; Beltran, H.; Cordoncillo, E.; West, A. R. *Inorg. Chem.* **2013**, *52*, 1729−1736.
(36) Rodríguez-Carvajal, J. *Newsletter* **2001**, *26*, 12−19.
(37) Dong, C. *J. Appl. Crystallogr.* **1999**, *32*, 838−838.
(38) Shannon, R. D. *Acta Crystallogr., Sect. A* **1976**, *32*, 751−767.
(39) Sciau, P.; Lu, Z.; Calvarin, G.; Roisnel, T.; Ravez, J. *Mater. Res. Bull.* **1993**, *28*, 1233−1239.
(40) Cohen, R. E. *Nature* **1992**, *358*, 136−138.
(41) Kuroiwa, Y.; Aoyagi, S.; Sawada, A.; Harada, J.; Nishibori, E.; Takata, M.; Sakata, M. *Phys. Rev. Lett.* **2001**, *87*, 217601−4.